

Emergence of d -orbital magnetic Dirac fermions in a MoS₂ monolayer with squared pentagon structure

Xuanyi Li,^{1,3} Sheng Meng,^{1,3,4,*} and Jia-Tao Sun^{2,1,†}

¹Beijing National Laboratory for Condensed Matter Physics and Institute of Physics, Chinese Academy of Sciences, Beijing 100190, China

²School of Information and Electronics, MIT Key Laboratory for Low-Dimensional Quantum Structure and Devices, Beijing Institute of Technology, Beijing 100081, China

³School of Physical Sciences, University of Chinese Academy of Sciences, Beijing 100049, China

⁴Songshan Lake Materials Laboratory, Dongguan, Guangdong 523808, China
and Collaborative Innovation Center of Quantum Matter, Beijing 100084, China



(Received 18 December 2019; accepted 12 March 2020; published 7 April 2020)

We find that an atomically thin MoS₂ monolayer with squared pentagon structure motifs, distinct from all the conventional MoS₂ monolayers, has unique electronic band structures with Dirac cones comprising d orbitals. The squared pentagon MoS₂ monolayer is an intrinsic ferromagnet with a high Curie temperature and behaves as a half semimetal, which possesses spin-polarized Dirac fermions around the Fermi level. Moreover, when spin-orbit couplings are included, the magnetic Dirac band is gapped, hosting quantized conductance channels. This work provides insights in achieving two-dimensional topological materials with unique atomistic patterns.

DOI: [10.1103/PhysRevB.101.144409](https://doi.org/10.1103/PhysRevB.101.144409)

I. INTRODUCTION

Since the discovery of a two-dimensional (2D) hexagonal carbon monolayer—graphene [1]—much attention has been drawn also to the topological properties of this class of materials. The intrinsic topological properties are determined by the singular point or nodal rings in the momentum space, such as the fourfold degeneracy Dirac points or the doubly degenerate Weyl points [2–5]. The well-known two-dimensional topological materials include the elemental materials (graphene [6], silicene [7], bismuthene [8], black phosphorus [9], etc.), binary compounds (SnSe [10], 1T'-WTe₂ [11], etc.), and their complex structures bonded together with substrates or molecular ligands [12–14]. Although many materials have been proposed to realize the quantum spin Hall effect (QSHE) or quantum anomalous Hall effect (QAHE) [15–17], the experimental realization of these proposals remains a great challenge. For example, graphene monolayer has been predicted to host the QSHE. However, due to the extremely weak spin-orbit coupling (SOC) in graphene, the predicted QSHE is only assumed to be realized at extremely low temperatures, which makes it infeasible in potential spintronic applications [18–22]. To have a larger SOC effect, it is of great interest to develop new materials comprising heavier elements or novel atomic arrangements.

Different from the conventional hexagonal structures, the squared 2D materials have received less attention. Only a few examples are reported. Recently, the squared transition metal dichalcogenides (TMDs) with pentagonal rings, such

as PdSe₂ and their polymorphs, have been experimentally realized [23,24]. Many studies show that PdSe₂ family compounds have new physics in “low-symmetry” structures, such as unique anisotropic electric conductivity and enhanced thermoelectricity, as well as potential applications in low-energy electronics or piezoelectrics [23–26]. In the PdSe₂ monolayer, the transition metal Pd atoms have four coordination with nonmetal atoms forming a buckled structure, indicating that PdSe₂ family are nonmagnetic. In general, currently most reported squared transition metal dichalcogenides are nonmagnetic. Therefore, it is interesting to find intrinsic magnetic 2D materials with a squared structure hosting the spin-polarized Dirac/Weyl fermions around the Fermi level [27–29]. Moreover, the PdSe₂ monolayer has a larger SOC effect due to the presence of heavy transition metal atoms. The d -orbital Dirac fermion with a stronger SOC effect within magnetic materials is promising to have QAHE with a larger topologically nontrivial energy gap [30].

Inspired by the squared PdSe₂ monolayer [31], we here report a unique squared structure of MoS₂ which is completely composed of planar pentagonal rings (named squared pentagon MoS₂, or sp -MoS₂) distinct from all the conventional hexagonal nonmagnetic TMDs. The half-metallic squared MoS₂ monolayer possesses intrinsic spin-polarized d -orbital Dirac cones, which are different from conventional Dirac cones contributed by p -orbital bands [6–8], or due to interfacial hybridization [12,30]. With spin-orbit couplings taken into account, a gap of 7.5 meV opens up in the magnetic Dirac band, which can host the quantized anomalous Hall effect [32]. Our work shows the peculiar magnetic and topological properties of alternative “low-symmetry” squared TMD monolayers beyond the conventional hexagonal nonmagnetic 2D materials.

* smeng@iphy.ac.cn

† jtsun@iphy.ac.cn

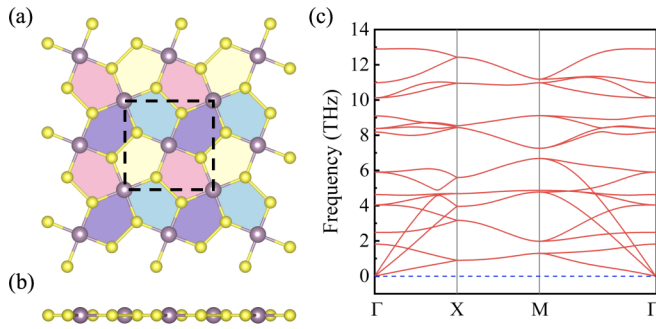


FIG. 1. Top view (a) and side view (b) of sp -MoS₂ monolayer. The squared unit cell is circled by the black dashed line. (c) The calculated phonon dispersion of sp -MoS₂.

II. CALCULATION METHODS

The first-principles calculations are performed on the basis of density functional theory (DFT [33,34]) as implemented in Vienna *ab initio* simulation package (VASP [35]) software. The generalized gradient approximation (GGA) proposed by Perdew, Burke, and Ernzerhof (PBE) [36] is used as the exchange-correlation functional. Ion cores are described by using the projector augmented wave (PAW [37,38]) method. A $10 \times 10 \times 1$ k -point grid generated by Monkhost-Pack is used in geometry relaxation, and the relaxation will only stop when the maximal Hellmann-Feynman force of all atoms is less than 10^{-3} eV/Å and free energy is less than 10^{-5} eV. The $50 \times 50 \times 1$ k point grid is used to obtain the density of states (DOS). The energy cutoff for the expansion of the plane wave basis is set to be 500 eV [39]. A vacuum of 20 Å is retained to avoid the interaction between periodic layers along the vertical direction. Spin-orbit coupling has been considered when calculating topological properties. The WANNIER90 package is used to get the fitted band structures of sp -MoS₂ monolayer from the Wannier basis. The wavefunction topology of sp -MoS₂ including Berry curvature and anomalous Hall conductivity is obtained on a very dense momentum grid of $900 \times 900 \times 1$ points [40,41]. The phonon dispersion of sp -MoS₂ is obtained by PHONOPY [42].

III. RESULTS AND DISCUSSION

The conventional layered transition metal dichalcogenides akin (but not limited) to MoS₂ have hexagonal structures with 1T, 2H, and 3R polymorphs respectively, which are composed of two sulfur sublayers located on both sides of the molybdenum atoms [43]. Distinct from the above, a squared pentagon phase of MoS₂ (sp -MoS₂) monolayer has been found here as shown in Figs. 1(a) and 1(b). The space group of sp -MoS₂ is $P4/mbm$ and its lattice constant is 6.04 Å. Four Mo-S bonds with the length of 2.33 Å and one S-S bond of 2.39 Å form a basic pentagon. There is no regular pentagon mosaic in nature, but the four adjacent pentagons here can form a squared cell to periodically tile the entire plane as the Cairo pentagonal tiling pattern [44]. All atoms are on the same plane, and a quadruple rotational symmetry exists, making this type of material different from the buckled pyrite monolayer such as PdSe₂ [23].

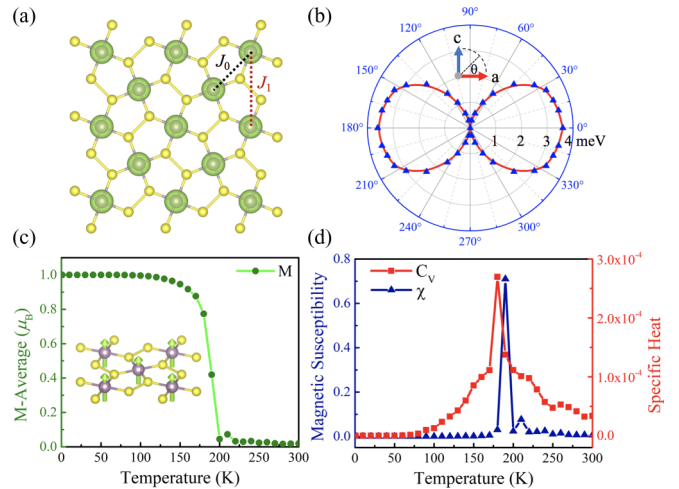


FIG. 2. (a) Top view of spin density distributions for the ferromagnetic sp -MoS₂ monolayer. The isosurface level is $0.01 \text{ eV}/\text{Å}^3$. (b) Calculated MAE by rotating the spin orientations within the x - z plane. (c) The simulated average magnetic moment as a dependence of temperature. The inset is the schematic diagram of one sp -MoS₂ unit cell. (d) The simulated magnetic susceptibility χ and specific heat C_V as a dependence of temperature.

To study the structural stability of the sp -MoS₂ monolayer, we first calculate the phonon dispersion. The 2D sheet of sp -MoS₂ is expanded into the $3 \times 3 \times 1$ supercell in order to approach the long-wavelength limit in the phonon dispersion. The phonon spectra of sp -MoS₂ shown in Fig. 1(c) have no imaginary frequency indicating its dynamical stability. We have also conducted *ab initio* molecular dynamics (AIMD) simulations, which last 5 ps with a time step of 1 fs. When the sp -MoS₂ monolayer is heated to near 300 K, the squared pentagon lattice can hold without significant atomic reconstructions.

To determine the magnetic structure of the sp -MoS₂, we perform spin-polarized density functional theory calculations by using a $2 \times 2 \times 1$ supercell. We have considered three different magnetic orderings, namely, ferromagnetic (FM), antiferromagnetic checkerboard (AFM-CB), and antiferromagnetic stripe (AFM-S) [27]. We also take into account the influence of Coulomb interaction on magnetic states by changing the on-site Coulomb (U) and exchange interactions (J) as in the Dudarev method [45]. The calculated total energies of the three magnetic structures of the sp -MoS₂ supercell under effective Coulomb interaction U_{eff} (the difference between U and J) show that the ferromagnetic state has the lowest energy, irrespective of any effective interaction U_{eff} . Figure 2(a) shows the spin density distributions of the ferromagnetic sp -MoS₂. It is obvious that the calculated magnetization densities are mainly localized on Mo atoms and the calculated magnetic moment is about $2 \mu_B$ per Mo atom. The magnetic anisotropy energy (MAE), which is defined as the energy difference between in-plane ($\theta = 0^\circ$) and out-of-plane ($\theta = 90^\circ$) spin orientations within the x - z plane, is shown in Fig. 2(b). We find that the out-of-plane magnetization direction is energetically preferred over the in-plane one by 3.6 meV per unit cell. Very dense momentum mesh is further considered to ensure the convergence of the calculated MAE.

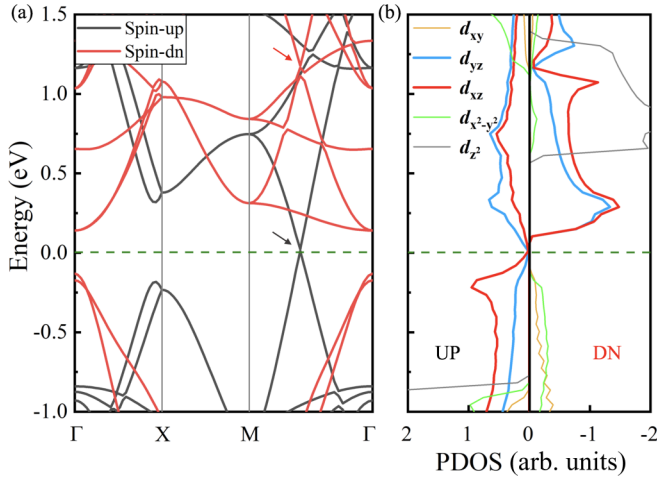


FIG. 3. (a) Spin-polarized band structures of a half-metallic sp -MoS₂ monolayer without spin-orbit coupling. The Dirac cones of spin-up (spin-dn) subbands at (above) the Fermi level are denoted by black (red) arrows. (b) Projected density of states on five d orbitals of Mo, indicating that the Dirac cone at the Fermi level is mainly contributed by Mo d_{xz} and d_{yz} orbitals.

To estimate the Curie temperature of the ferromagnetic sp -MoS₂ monolayer, we conduct Monte Carlo simulations based on a two-dimensional Heisenberg model in view of its out-of-plane magnetization direction [46]. The Hamiltonian of the 2D Heisenberg model is

$$H = \sum_{\langle i,j \rangle} J_0 \mathbf{S}_i \cdot \mathbf{S}_j + \sum_{\langle\langle i,j \rangle\rangle} J_1 \mathbf{S}_i \cdot \mathbf{S}_j + \sum_i D S_i^2, \quad (1)$$

where J_0 (J_1) and D describe the strength of isotropic symmetric exchange interactions and single ion anisotropy, respectively. According to the magnetic structure of sp -MoS₂ in Fig. 2(a), each spin \mathbf{S}_i has four nearest neighbors \mathbf{S}_j , constructing a square grid. In principle, J_0 (J_1) is determined by the energy difference caused by one nearest (next-nearest) pair of $\mathbf{S}_i \cdot \mathbf{S}_j$ interactions inverting from spin parallel to spin antiparallel, which is obtained by comparing the total energies between the FM and AFM-CB states. Coefficient D is determined by the MAE between in-plane and out-of-plane directions, which has a negligible effect on the Curie temperature because of the dominated intrinsic isotropic ferromagnetism. The Monte Carlo simulations are performed on a 100×100 lattice grid lasting for 5 000 000 steps with a step size of 10 K. The obtained Curie temperature of sp -MoS₂ is 190 K as shown in Figs. 2(c) and 2(d), where the magnetic susceptibility χ and the specific heat C_V are both considered to improve the estimation accuracy. The AIMD simulations show that the magnetic state of sp -MoS₂ can remain under 200 K, which is comparable with the obtained Curie temperature by Monte Carlo simulations. Considering that the Monte Carlo simulations of Heisenberg models usually overestimate the real Curie temperature, the calculated 190 K here can be taken as an upper limit.

The spin-polarized electronic structures of the sp -MoS₂ monolayer are presented in Fig. 3(a). It is found that the spin-up subbands cross the Fermi level while the spin-down subbands are gapped indicating its half-metallic behavior [47].

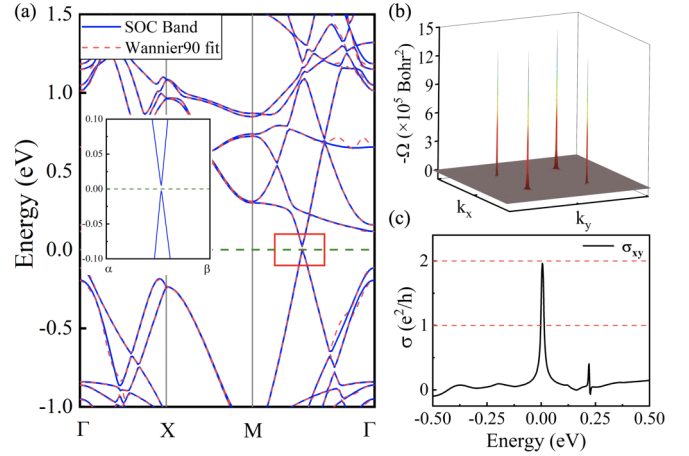


FIG. 4. (a) Electronic structures (blue lines) and Wannier basis fitting (red dashes) of sp -MoS₂ with SOC. The inset shows the band structure in the energy range from -0.1 to 0.1 eV along the M - Γ direction. (b) Berry curvature and (c) anomalous Hall conductivity of the sp -MoS₂ monolayer with SOC.

Further inspection shows that the spin-up subbands display semimetallic linear dispersion around the Fermi level similar to the Dirac cone in the graphene monolayer. Coincidentally, we find the same linear dispersion of spin-down subbands with an exchange energy splitting of 1.16 eV away from the Fermi level, indicating that two spin-polarized Dirac cones exist in magnetic sp -MoS₂. The projected density of states (PDOS) in Fig. 3(b) shows that the linear dispersion of spin-up subbands is dominated by Mo d_{xz} and d_{yz} orbitals. Therefore, the Dirac bands given here are intrinsically different from the p_z orbital of group-IV_A elemental monolayers such as graphene or silicene [6–8]. It is also remarkably distinct with those extrinsic ones due to the interfacial hybridization [12,30].

After the inclusion of the SOC, the Dirac cone of sp -MoS₂ around the Fermi level opens a gap of 7.5 meV, which is several orders of magnitude larger than that of graphene [48]. Because of the time-reversal symmetry breaking and the SOC gap, the QAHE is expected in the sp -MoS₂ monolayer. To confirm this point, we first fit a tight-binding (TB) model Hamiltonian with maximally localized Wannier functions to the PBE band structures by using the WANNIER90 package. The Mo d orbitals and S p orbitals are taken into account to fit the DFT band structures of sp -MoS₂. Figure 4(a) shows that the calculated band structures in the Wannier basis set are in good agreement with the PBE results, especially around the Fermi level. The QAHE is further demonstrated by calculating the first Chern number,

$$C = \frac{1}{2\pi} \sum_n \int_{\text{BZ}} d^2k \Omega_n, \quad (2)$$

where Ω_n is the momentum-space Berry curvature [49–51] for the n th band which contributes to the spin-polarized Dirac cone:

$$\Omega_n(k) = - \sum_{n' \neq n} \frac{2\text{Im} \langle \psi_{nk} | v_x | \psi_{n'k} \rangle \langle \psi_{n'k} | v_y | \psi_{nk} \rangle}{(\epsilon_{n'} - \epsilon_n)^2}. \quad (3)$$

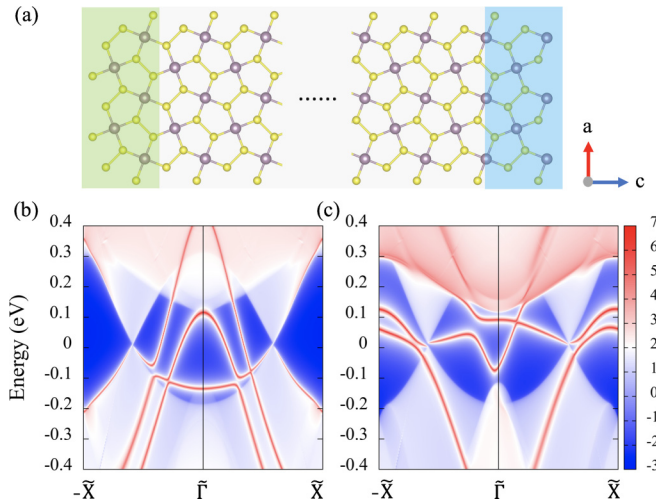


FIG. 5. (a) The nanoribbon structure of the sp -MoS₂ monolayer. Green and blue regions represent the left and right edges of the sp -MoS₂ nanoribbon, respectively. Topology calculations on left (b) and right (c) edges of the nanoribbon show two topological chiral edge states cross the Fermi level.

The calculated Berry curvature in the first Brillouin zone is shown in Fig. 4(b). The Berry curvature distribution, which is also known as magnetic monopole in the momentum space, has four sharp spikes corresponding to the position of the four Dirac points. By integrating the Berry curvature $\Omega_n(k)$ in the entire Brillouin zone, we get the anomalous Hall conductivity as $370(\Omega \text{ cm})^{-1}$, which closely corresponds to the Chern number $\mathcal{C} = -2$. As we know that each Dirac cone gives rise to $|\mathcal{C}| = 1/2$, the four positive spikes accurately reproduce the total Chern number. Moreover, the calculated quantum anomalous Hall conductivity in Fig. 4(c) also proves that the sp -MoS₂ monolayer is a quantum anomalous Hall phase. Therefore, two topological nontrivial chiral edge states will occur crossing the Fermi surface.

To confirm these significant features of QAHE, we build a nanoribbon with the width of 20 unit cells, shown in Fig. 5(a),

to examine the topological edge states of sp -MoS₂. The width of the nanoribbon is 120 Å, which is large enough to avoid interactions between the opposite edges. The electronic states of the left and right edges of the sp -MoS₂ nanoribbon are shown in Figs. 5(b) and 5(c). Two topological chiral edge states go across the Fermi level, in agreement with the calculated Chern number $\mathcal{C} = -2$. The certified spin-polarized Dirac fermion is consistent with nontrivial topological characters, suggesting that the sp -MoS₂ monolayer proposed here is an intrinsic single spin magnetic topological insulator, which holds great promise for generating QAHE.

IV. CONCLUSION

In conclusion, through first-principles calculations we predict a unique squared pentagon phase of a MoS₂ monolayer, which is different from the widely studied hexagonal MoS₂ phases. The sp -MoS₂ monolayer is confirmed to be a half semimetal with a high Curie temperature (~ 190 K), which has a ferromagnetic ground state and isotropic out-of-plane magnetic direction. The spin-polarized Dirac cone at the vicinity of the Fermi level is mainly contributed by d_{xz} and d_{yz} orbitals of Mo, radically distinct from the Dirac fermions composed by p orbitals. As a result, the intrinsic strong SOC of d electrons will open a topological nontrivial gap endowing the sp -MoS₂ with the QAHE phase. The theoretical predictions on the sp -MoS₂ monolayer may stimulate experimental efforts to manufacture magnetic materials with dissipationless conductance channels.

ACKNOWLEDGMENTS

This work is financially supported by the National Key Research and Development Program of China (Grants No. 2016YFA0202300 and No. 2016YFA0300902), National Natural Science Foundation of China (Grants No. 91850120 and No. 11974045), and ‘‘Strategic Priority Research Program (B)’’ of Chinese Academy of Sciences (Grant No. XDB30000000). The computing resources were provided by Songshan Lake supercomputing facilities.

- [1] K. S. Novoselov, A. K. Geim, S. V. Morozov, D. Jiang, Y. Zhang, S. V. Dubonos, I. V. Grigorieva, and A. A. Firsov, *Science* **306**, 666 (2004).
- [2] Z. K. Liu, B. Zhou, Y. Zhang, Z. J. Wang, H. M. Weng, D. Prabhakaran, S. Mo, Z. X. Shen, Z. Fang, X. Dai, Z. Hussain, and Y. L. Chen, *Science* **343**, 864 (2014).
- [3] B. Q. Lv, H. M. Weng, B. B. Fu, X. P. Wang, H. Miao, J. Ma, P. Richard, X. C. Huang, L. X. Zhao, G. F. Chen, Z. Fang, X. Dai, T. Qian, and H. Ding, *Phys. Rev. X* **5**, 031013 (2015).
- [4] N. P. Armitage, E. J. Mele, and A. Vishwanath, *Rev. Mod. Phys.* **90**, 015001 (2018).
- [5] H. Weng, X. Dai, and Z. Fang, *J. Phys.: Condens. Matter* **28**, 303001 (2016).
- [6] A. H. Castro Neto, F. Guinea, N. M. R. Peres, K. S. Novoselov, and A. K. Geim, *Rev. Mod. Phys.* **81**, 109 (2009).
- [7] S. Cahangirov, M. Topsakal, E. Aktürk, H. Şahin, and S. Ciraci, *Phys. Rev. Lett.* **102**, 236804 (2009).
- [8] M. Pumera and Z. Sofer, *Adv. Mater.* **29**, 1605299 (2017).
- [9] H. Liu, J. T. Sun, C. Cheng, F. Liu, and S. Meng, *Phys. Rev. Lett.* **120**, 237403 (2018).
- [10] Y. Sun, Z. Zhong, T. Shirakawa, C. Franchini, D. Li, Y. Li, S. Yunoki, and X. Q. Chen, *Phys. Rev. B* **88**, 235122 (2013).
- [11] F. Zheng, C. Cai, S. Ge, X. Zhang, X. Liu, H. Lu, Y. Zhang, J. Qiu, T. Taniguchi, K. Watanabe, S. Jia, J. Qi, J. H. Chen, D. Sun, and J. Feng, *Adv. Mater.* **4845** (2016).
- [12] H. Fu, Z. Liu, C. Lian, J. Zhang, H. Li, J. T. Sun, and S. Meng, *Phys. Rev. B* **94**, 035427 (2016).
- [13] Z. F. Wang, Z. Liu, and F. Liu, *Phys. Rev. Lett.* **110**, 196801 (2013).
- [14] Z. F. Wang, K. H. Jin, and F. Liu, *Wiley Interdiscip. Rev.: Comput. Mol. Sci.* **7**, e1304 (2017).
- [15] C. Z. Chang, J. Zhang, X. Feng, J. Shen, Z. Zhang, M. Guo, K. Li, Y. Ou, P. Wei, L. L. Wang, Z. Q. Ji, Y. Feng, S. Ji, X. Chen, J. Jia, X. Dai, Z. Fang, S. C. Zhang, K. He, Y. Wang *et al.*, *Science* **340**, 167 (2013).

- [16] R. Yu, W. Zhang, H.-J. Zhang, S.-C. Zhang, X. Dai, and Z. Fang, *Science* **329**, 61 (2010).
- [17] X.-L. Qi and S.-C. Zhang, *Rev. Mod. Phys.* **83**, 1057 (2011).
- [18] C. Cheng, J. T. Sun, X. R. Chen, and S. Meng, *Sci Bull.* **63**, 85 (2018).
- [19] Y. Zhang, Y. W. Tan, H. L. Stormer, and P. Kim, *Nature* **438**, 201 (2005).
- [20] K. S. Novoselov, A. K. Geim, S. V. Morozov, D. Jiang, M. I. Katsnelson, I. V. Grigorieva, S. V. Dubonos, and A. A. Firsov, *Nature* **438**, 197 (2005).
- [21] K. I. Bolotin, F. Ghahari, M. D. Shulman, H. L. Stormer, and P. Kim, *Nature* **462**, 196 (2009).
- [22] X. Du, I. Skachko, F. Duerr, A. Luican, and E. Y. Andrei, *Nature* **462**, 192 (2009).
- [23] A. D. Oyedele, S. Yang, L. Liang, A. A. Puzdov, K. Wang, J. Zhang, P. Yu, P. R. Pudasaini, A. W. Ghosh, Z. Liu, C. M. Rouleau, B. G. Sumpter, M. F. Chisholm, W. Zhou, P. D. Rack, D. B. Geohegan, and K. Xiao, *J. Am. Chem. Soc.* **139**, 14090 (2017).
- [24] E. Li, D. Wang, P. Fan, R. Zhang, Y. Y. Zhang, G. Li, J. Mao, Y. Wang, X. Lin, S. Du, and H. J. Gao, *Nano Res.* **11**, 5858 (2018).
- [25] Y. Ma, L. Kou, X. Li, Y. Dai, and T. Heine, *NPG Asia Mater.* **8**, e264 (2016).
- [26] J. Sun, H. Shi, T. Siegrist, and D. J. Singh, *Appl. Phys. Lett.* **107**, 153902 (2015).
- [27] H. Liu, J. T. Sun, M. Liu, and S. Meng, *J. Phys. Chem. Lett.* **9**, 6709 (2018).
- [28] W. Li, M. Guo, G. Zhang, and Y. W. Zhang, *Phys. Rev. B* **89**, 205402 (2014).
- [29] J. Wang, S. Deng, Z. Liu, and Z. Liu, *Natl. Sci. Rev.* **2**, 22 (2015).
- [30] Y. Li, P. Tang, P. Chen, J. Wu, B. L. Gu, Y. Fang, S. B. Zhang, and W. Duan, *Phys. Rev. B* **87**, 245127 (2013).
- [31] S. Haastrup, M. Strange, M. Pandey, T. Deilmann, P. S. Schmidt, N. F. Hinsche, M. N. Gjerding, D. Torelli, P. M. Larsen, A. C. Riis-Jensen, J. Gath, K. W. Jacobsen, J. J. Mortensen, T. Olsen, and K. S. Thygesen, *2D Mater.* **5**, 042002 (2018).
- [32] X. L. Sheng, Z. M. Yu, R. Yu, H. Weng, and S. A. Yang, *J. Phys. Chem. Lett.* **8**, 3506 (2017).
- [33] P. Hohenberg and W. Kohn, *Phys. Rev.* **136**, B864 (1964).
- [34] W. Kohn and L. J. Sham, *Phys. Rev.* **140**, A1133 (1965).
- [35] G. Kresse and J. Furthmüller, *Phys. Rev. B* **54**, 11169 (1996).
- [36] J. P. Perdew, K. Burke, and M. Ernzerhof, *Phys. Rev. Lett.* **77**, 3865 (1996).
- [37] P. E. Blöchl, *Phys. Rev. B* **50**, 17953 (1994).
- [38] M. Gajdoš, K. Hummer, G. Kresse, J. Furthmüller, and F. Bechstedt, *Phys. Rev. B* **73**, 045112 (2006).
- [39] J. Paier, R. Hirschl, M. Marsman, and G. Kresse, *J. Chem. Phys.* **122**, 234102 (2005).
- [40] G. Pizzi, V. Vitale, R. Arita, S. Blügel, F. Freimuth, G. Géranton, M. Gibertini, D. Gresch, C. Johnson, T. Koretsune, J. Ibañez-Azpiroz, H. Lee, J.-M. Lihm, D. Marchand, A. Marrazzo, Y. Mokrousov, J. I. Mustafa, Y. Nohara, Y. Nomura, L. Paulatto, S. Poncé, T. Ponweiser, J. Qiao, F. Thöle, S. S. Tsirkin, M. Wierzbowska, N. Marzari, D. Vanderbilt, I. Souza, A. A. Mostofi, and J. R. Yates, *J. Phys. Cond. Matt.* **32**, 165902 (2020).
- [41] Q. S. Wu, S. N. Zhang, H. F. Song, M. Troyer, and A. A. Soluyanov, *Comput. Phys. Commun.* **224**, 405 (2018).
- [42] A. Togo and I. Tanaka, *Scr. Mater.* **108**, 1 (2015).
- [43] K. F. Mak, C. Lee, J. Hone, J. Shan, and T. F. Heinz, *Phys. Rev. Lett.* **105**, 136805 (2010).
- [44] E. Ressouche, V. Simonet, B. Canals, M. Gospodinov, and V. Skumryev, *Phys. Rev. Lett.* **103**, 267204 (2009).
- [45] S. Lutfalla, V. Shapovalov, and A. T. Bell, *J. Chem. Theory Comput.* **7**, 2218 (2011).
- [46] J. Liu, M. Shi, J. Lu, and M. P. Anantram, *Phys. Rev. B* **97**, 054416 (2018).
- [47] R. A. de Groot, F. M. Mueller, P. G. van Engen, and K. H. J. Buschow, *Phys. Rev. Lett.* **50**, 2024 (1983).
- [48] Y. Yao, F. Ye, X.-L. Qi, S.-C. Zhang, and Z. Fang, *Phys. Rev. B* **75**, 041401(R) (2007).
- [49] D. J. Thouless, M. Kohmoto, M. P. Nightingale, and M. den Nijs, *Phys. Rev. Lett.* **49**, 405 (1982).
- [50] M. C. Chang and Q. Niu, *Phys. Rev. Lett.* **75**, 1348 (1995).
- [51] Y. Yao, L. Kleinman, A. H. MacDonald, J. Sinova, T. Jungwirth, D. S. Wang, E. Wang, and Q. Niu, *Phys. Rev. Lett.* **92**, 037204 (2004).